

Monte-Carlo closure for moment-based transport schemes in general relativistic radiation hydrodynamics simulations

Francois Foucart^{1,2} 

¹ Lawrence Berkeley National Laboratory, 1 Cyclotron Rd, Berkeley, CA 94720, USA

² Department of Physics, University of New Hampshire, Durham, New Hampshire 03824, USA

Accepted XXX. Received YYY; in original form ZZZ

ABSTRACT

General relativistic radiation hydrodynamics simulations are necessary to accurately model a number of astrophysical systems involving black holes and neutron stars. Photon transport plays a crucial role in radiatively dominated accretion disks, while neutrino transport is critical to core-collapse supernovae and to the modeling of electromagnetic transients and nucleosynthesis in neutron star mergers. However, evolving the full Boltzmann equations of radiative transport is extremely expensive. We describe the implementation of a cheaper general relativistic radiation hydrodynamics method which explicitly converges to a solution of Boltzmann’s equation in the limit of infinite numerical resources. The algorithm is based on a gray two-moment scheme, in which we evolve the energy density and momentum density of the radiation. Two-moment schemes require a closure which fills in missing information about the energy spectrum and higher-order moments of the radiation. Instead of the approximate analytical closure currently used in core-collapse and merger simulations, we complement the two-moment scheme with a low-accuracy Monte-Carlo evolution. We describe how the two algorithms are coupled for self-consistent evolutions, and present a set of test problems demonstrating the reliability of our implementation of that algorithm in the general relativistic SpEC code, and its current limitations. We expect these methods to allow for greatly improved accuracy in the evolution of neutrinos in neutron star merger simulations. Our algorithm can also be useful in radiation hydrodynamics simulations of other general relativistic systems.

Key words: Radiation transport – Black holes – Neutron Stars – Numerical Methods – General Relativity

1 INTRODUCTION

Neutrinos and photons play a critical role in numerical studies of astrophysical systems. In particular, general relativistic photon transport is required to study radiatively dominated accretion disks, while neutrino-matter interactions are crucial to the explosion mechanism of core-collapse supernovae. In neutron star mergers, neutrinos do not directly affect the dynamics of the merger, yet they are the main source of cooling of the accretion disks and massive neutron stars formed as a result of many mergers. Neutrino-matter interactions also determine the evolution of the composition of the matter ejected by these mergers. These neutron-rich outflows undergo rapid neutron capture (r-process) nucleosynthesis, making mergers promising candidates as the site of production of many heavy elements (e.g. gold, platinum, uranium, Korobkin et al. 2012; Wanajo et al.

2014). Radioactive decay of the ashes of the r-process also power maybe the most promising electromagnetic counterparts to the gravitational waves emitted by the mergers: the optical/infrared transients called *kilonovae* (Lattimer & Schramm 1976; Li & Paczynski 1998; Roberts et al. 2011; Kasen et al. 2013). The mass and composition of these outflows are the main determinant of the color, duration, and luminosity of kilonovae (Barnes & Kasen 2013), while the composition of the outflows largely set the relative yields of different heavy elements as a result of r-process nucleosynthesis (Korobkin et al. 2012; Wanajo et al. 2014; Lippuner & Roberts 2015). Accordingly, neutrino transport is an important component in any effort to model kilonovae and r-process nucleosynthesis in mergers. Neutrino-antineutrino annihilation can also deposit a significant amount of energy in low-density regions above the remnant (Perego et al. 2017). While, on their own, $\nu\bar{\nu}$ annihilation probably do not deposit enough energy to power short gamma-ray bursts (SGRBs) in merger remnants, they may help their produc-

* fv Foucart@lbl.gov

tion by clearing the polar regions of baryonic matter (Fujibayashi et al. 2017).

The main objective of a radiation transport scheme is to evolve the distribution function $f_{(\nu)}(x^\mu, p^\mu)$ of neutrinos or photons, where $x^\mu = (t, x^i)$ are the spacetime coordinates and $p^\mu = dx^\mu/d\lambda$ is the 4-momentum of the neutrinos/photons, with λ some affine parameter. As we neglect neutrino masses, the 4-momentum is a null vector, i.e. $p^\mu p_\mu = 0$. The distribution function of photons and of each species of neutrinos evolves according to Boltzmann's equation

$$p^\alpha \left[\frac{\partial f_{(\nu)}}{\partial x^\alpha} - \Gamma_{\alpha\gamma}^\beta p^\gamma \frac{\partial f_{(\nu)}}{\partial p^\beta} \right] = \left[\frac{df_{(\nu)}}{d\tau} \right]_{\text{coll}}, \quad (1)$$

where $\Gamma_{\beta\gamma}^\alpha$ are the Christoffel symbols and the right-hand side includes all collisional processes. Solving Boltzmann's equation thus requires the evolution in time of a 6-dimensional function, a very steep computational challenge. The main objective of this work is to provide a relatively cheap algorithm for general relativistic radiation transport which, while approximate for the numerical resolution that we can current afford, asymptotes to Boltzmann's equation in the limit of infinite computational resources. While the algorithm is generally applicable to any problem involving general relativistic photon or neutrino transport, we implement and test it with the problem of neutrino transport in merger simulations in mind. We implement the algorithm in the SpEC code¹, currently used to study merging black holes and neutron stars.

In the context of neutron star-neutron star (NSNS) and neutron star-black hole (NSBH) mergers, neutrinos have so far been handled using approximate transport schemes, with sophistication ranging from order-of-magnitude accurate leakage schemes (Deaton et al. 2013; Neilsen et al. 2014), to various moment schemes in which only the lowest or two-lowest moments of $f_{(\nu)}$ in momentum space are evolved (Wanajo et al. 2014; Foucart et al. 2015; Radice et al. 2016). In both cases, neutrino transport has generally been performed in the gray approximation, in which information about the neutrino spectrum is either unavailable or, in the case of our most recent moment scheme, reduced to the knowledge of the average energy of the neutrinos (Foucart et al. 2016b). Spectral (energy-dependent) leakage and moment schemes have been used in Newtonian simulations of post-merger accretion disks (Just et al. 2015; Perego et al. 2016), or in the context of core-collapse supernovae (Roberts et al. 2016), but not for NSNS/NSBH mergers. This is particularly problematic because neutrino cross-sections have a strong dependence in the energy of neutrinos. In fact, we have already demonstrated in the context of NSNS mergers that most, if not all, schemes used by current codes lead to significant errors in the computation of the composition of the ejecta (Foucart et al. 2016a,b).

Moment schemes require information about moments of $f_{(\nu)}$ which are not evolved in the simulation. For example, in the two-moment formalism, the energy and flux density of the neutrinos are evolved, and the evolution equations require information about the pressure tensor of the neutrinos. Semi-arbitrary choices have to be made to close the evolution equations. The most common choice in recent simulations

has been to use a two-moment scheme with the Minerbo (M1) closure (Minerbo 1978), which is only well-defined in the optically thick limit and for a single beam of neutrinos in the optically thin limits. In other regimes, the closure is inaccurate. The best known consequence of this choice of closure is the presence of radiation shocks whenever neutrino beams cross or converge.

To go beyond the moment formalism, at least two directions can be considered. The first is to discretize $f_{(\nu)}$ in momentum space. The cost associated with a 6-dimensional grid is however prohibitive. Recently, a first axisymmetric simulation with a full discretization of $f_{(\nu)}$ has been performed in the context of core-collapse supernovae (Nagakura et al. 2017). While such a scheme may one day become affordable without reducing the dimensionality of the problem, it remains at this point well beyond our reach. The second choice is to rely on Monte-Carlo (MC) methods, which randomly sample the 6-dimensional space of $f_{(\nu)}$. In MC codes, we evolve *neutrino packets* which each represent large numbers of neutrinos and propagate through the numerical grid. The distribution $f_{(\nu)}$ can be reconstructed at any point from these packets, within statistical errors due to the finite number of samples. Recently, the MC code *Sedonu* has been used to perform Newtonian evolutions of the neutrinos in time-independent snapshots of supernovae simulations (Richers et al. 2017), while the general relativistic code *bhlight* has been developed for simulations of accretion disks (Ryan et al. 2015). While 6-dimensional general relativistic simulations of neutrino transport coupled to general relativistic hydrodynamics simulations of supernovae or neutron star mergers with an MC code appear closer than with a grid-based code, they still require a very significant investment of computational resources.

In this paper, we present the first implementation in a general relativistic hydrodynamics code of a somewhat cheaper option: using a moment scheme in which unknown moments of $f_{(\nu)}$ and neutrino spectra are obtained from a MC evolution of the neutrinos. Our method is developed in the spirit of the Variable Eddington Tensor algorithm implemented in the Athena code by Davis et al. (2012) for Newtonian simulations of accretion disks, except that we use the noisier but cheaper Monte-Carlo methods to provide the closure instead of the short-characteristic method used by Davis et al. (2012).

The fact that we have to evolve neutrinos with a MC scheme may give the impression that our algorithm does not provide any advantage over a pure MC evolution. However, using MC only as a way to close the equations for the evolution of the moments allows us to take two important, cost-saving shortcuts. First, we use MC to compute time-averaged moments of $f_{(\nu)}$. At fixed number of neutrino packets on the grid, this allows us to reduce the statistical error in the computation of the moments of $f_{(\nu)}$ without increasing the cost of the simulation. This comes, however, at the cost of smoothing over time the value of these moments. Second, we can completely side-step a common issue in MC simulations: the high cost of evolving optically thick regions, in which many packets are constantly created and reabsorbed. MC codes can partially avoid this issue by switching to a different treatment of the neutrinos in optically thick regions, e.g. by using MC methods to approximate a diffusion equation through optically thick regions. We simply rely on the

¹ <http://www.black-holes.org/SpEC.html>

moment scheme in optically thick regions, where it is very accurate, and only evolve MC packets below a certain optical depth. Additionally, we note that the use of a moment scheme avoids the risk of large swings in the temperature, composition, or velocity of the fluid which can occur in pure MC codes when a packet is absorbed or scattered in low-density regions, where the energy of a packet can be comparable to or larger than the energy of the fluid within a grid cell. Finally, because the MC evolution asymptotes to the exact solution of Boltzmann's equation, and the closure in the moment equations is now directly taken from that solution, the algorithm satisfies our requirement that it will converge to a true solution of the transport problem as more computational resources become available.

We structure the paper as follow. First, we describe the MC and moment schemes implemented in SpEC. Then, we discuss how the coupling between the two schemes and the coupling of the neutrinos to the general relativistic hydrodynamics simulation is handled. We also present a series of code tests demonstrating the ability of our algorithm to properly evolve the general relativistic equations of radiation transport, alone or coupled to the evolution of the temperature and composition of a background fluid. Finally, we discuss prospects for the use of that scheme in future simulations of neutron star mergers.

In the rest of this paper, we assume that $G = c = 1$. For subscripts and superscripts, greek letters are spacetime indices going from 0 to 3, and roman letters are spatial indices going from 1 to 3. When a black hole is involved in the simulation its mass is $M_{\text{BH}} = 1$. Otherwise, we work with an arbitrary mass unit $M = 1$ (code units), or with $M_{\odot} = 1$.

2 NUMERICAL METHODS

2.1 Definitions and reference frames

The SpEC code can be used to evolve Einstein's equations of general relativity coupled to the general relativistic equations of hydrodynamics. In this paper, however, we focus on the development of a new neutrino transport scheme for SpEC. For the code tests presented here, we do not evolve Einstein's equations, while the fluid is at most evolved through its coupling to the neutrinos. From our experience developing a two-moment neutrino transport scheme in SpEC, we do not expect the full coupling to Einstein's equations and the equations of hydrodynamics to create new problems in our evolutions, although whether this remain true for the coupled MC-moment scheme developed here remains to be tested in practice.

We assume a 3+1 decomposition of spacetime. The 3+1 decomposition relies on a foliation of spacetime into slices of constant time coordinate t , with timelike unit normal $n^{\mu} = \alpha^{-1}(t^{\mu} - \beta^{\mu})$ and line element

$$\begin{aligned} ds^2 &= g_{\mu\nu} dx^{\mu} dx^{\nu} \\ &= -\alpha^2 dt^2 + \gamma_{ij} (dx^i + \beta^i dt)(dx^j + \beta^j dt), \end{aligned} \quad (2)$$

where $g_{\mu\nu}$ is the 4-metric, γ_{ij} the 3-metric on a slice of constant t , α the lapse, and β^i the shift vector. Our numerical grid is discretized in the spatial coordinates x^i . We will refer to the coordinates (t, x^i) as the *grid frame*.

The fluid is described by its baryon density ρ , temperature T , electron fraction Y_e , and 4-velocity u^{μ} . Two special observers will play an important role in the description of our neutrino transport algorithm: *inertial observers*, whose timeline is tangent to n^{μ} , and *comoving observers*, whose timeline is tangent to u^{μ} . We also define the *comoving coordinates* (t', x'^i) , which are defined at a point so that

$$ds^2 = \eta_{\mu'\nu'} dx^{\mu'} dx^{\nu'}, \quad (3)$$

with $\eta_{\mu\nu}$ the Minkowski metric, and $(t')^{\mu} = u^{\mu}$. We construct these coordinates from an orthonormal tetrad $\hat{e}_{\mu}^{(\lambda')}$, with $g^{\mu\nu} \hat{e}_{\mu}^{(\lambda')} \hat{e}_{\nu}^{(\kappa')} = \eta^{\lambda'\kappa'}$, and $\hat{e}_{(t')}^{\mu} = u^{\mu}$. The three other components of the tetrad are obtained by applying Gram-Schmidt's algorithm to the vectors $e_{(i)}^{\mu} = \delta_i^{\mu}$, for $i = 1, 2, 3$. The orthonormal tetrad $\hat{e}_{(\lambda')}^{\mu}$ and the corresponding one-forms $\hat{e}_{\mu}^{(\lambda')}$ are precomputed and stored for each grid cell, and can be used to easily perform transformations from comoving coordinates to grid coordinates (and vice-versa) by simple matrix-vector multiplications.

Unless otherwise specified, vector and tensor components are expressed in the grid coordinates. The comoving coordinates are mostly used to compute neutrino-matter interactions. Quantities expressed in comoving coordinates will be primed, e.g. $p^{\mu'}$ for the momentum of the neutrinos in comoving coordinates.

2.2 Two-moments transport

The first layer of our transport scheme is based on the two-moment formalism, which we already implemented in the SpEC code and used for the study of NSBH (Foucart et al. 2015) and NSNS (Foucart et al. 2016a,b) mergers. The general idea of the scheme, proposed by Thorne (1981) and Shibata et al. (2011), is to evolve moments of the distribution function $f_{(\nu)}$. These can be defined from the stress-energy tensor of the neutrinos,

$$T_{(\nu)}^{\mu\nu} = E n^{\mu} n^{\nu} + F^{\mu} n^{\nu} + n^{\mu} F^{\nu} + P^{\mu\nu}. \quad (4)$$

Here, E is the energy density of the neutrinos measured by an inertial observer. The energy flux F^{μ} and pressure tensor $P^{\mu\nu}$ are both normal to n^{μ} , i.e. $F^{\mu} n_{\mu} = P^{\mu\nu} n_{\mu} = P^{\mu\nu} n_{\nu} = 0$. Evolution equations for $\tilde{E} = \sqrt{\gamma} E$, $\tilde{F}_i = \sqrt{\gamma} F_i$, with γ the determinant of the 3-metric γ_{ij} , are obtained by integrating Boltzmann's equation:

$$\partial_t \tilde{E} + \partial_j (\alpha \tilde{F}^j - \beta^j \tilde{E}) \quad (5)$$

$$= \alpha (\tilde{P}^{ij} K_{ij} - \tilde{F}^j \partial_j \ln \alpha - \tilde{S}^{\alpha} n_{\alpha}),$$

$$\partial_t \tilde{F}_i + \partial_j (\alpha \tilde{P}_i^j - \beta^j \tilde{F}_i) \quad (6)$$

$$= (-\tilde{E} \partial_i \alpha + \tilde{F}_k \partial_i \beta^k + \frac{\alpha}{2} \tilde{P}^{jk} \partial_i \gamma_{jk} + \alpha \tilde{S}^{\alpha} \gamma_{i\alpha}),$$

where K_{ij} is the extrinsic curvature of the current spatial slice. To close this system of equations, we require two pieces of information: the pressure $\tilde{P}_{ij} = \sqrt{\gamma} P_{ij}$ and the source terms $\tilde{S}^{\alpha} = \sqrt{\gamma} S^{\alpha}$. We define

$$P_{ij} = \pi_{ij} E, \quad (7)$$

$$S^{\alpha} = \eta u^{\alpha} - \kappa_{\alpha} J u^{\alpha} - (\kappa_{\alpha} + \kappa_s) H^{\alpha}, \quad (8)$$

where the Eddington tensor π_{ij} , the absorption opacity κ_{α} , and the scattering opacity κ_s are quantities to be provided by

the MC code, while the emissivity η is taken from tabulated values for neutrino-matter interactions (see Sec. 2.4). The moments J and H^α are, respectively, the energy density and flux density measured by a comoving observer, which can be defined from the stress-energy tensor of the neutrinos

$$T_{(\nu)}^{\mu\nu} = Ju^\mu u^\nu + H^\mu u^\nu + u^\mu H^\nu + S^{\mu\nu}, \quad (9)$$

with $S^{\mu\nu}$ the pressure tensor in the fluid frame, $H^\mu u_\mu = S^{\mu\nu} u_\mu = S^{\mu\nu} u_\nu = 0$. J and H^μ can thus be computed as functions of E , F_i , and π_{ij} , by taking projections of $T_{(\nu)}^{\mu\nu}$.

An equivalent, and more intuitive definition of the moments is to start from the comoving moments

$$J = \int d\nu v^3 \int d\Omega f_{(\nu)} \quad (10)$$

$$H^\mu = \int d\nu v^3 \int d\Omega f_{(\nu)} l^\mu \quad (11)$$

$$S^{\mu\nu} = \int d\nu v^3 \int d\Omega f_{(\nu)} l^\mu l^\nu \quad (12)$$

with ν the neutrino energy in the fluid frame, $\int d\Omega$ integrals over solid angle on a unit sphere in momentum space, and

$$p^\mu = \nu(l^\mu + l^\mu), \quad (13)$$

the 4-momentum of neutrinos, with $l^\mu u_\mu = 0$.

We use high-order finite volume methods to evolve (\tilde{E}, \tilde{F}_i) . A locally implicit time stepping allows us to handle stiff neutrino-matter interaction terms, while the flux terms are computed explicitly. The only terms to be treated implicitly in the equations are those containing the source terms S^α . Thanks to the linearity of the equations in (\tilde{E}, \tilde{F}_i) , we can solve the implicit problem exactly by inverting a 4×4 matrix for each neutrino species at each point.

In practice, we compute the fluxes $(\alpha \tilde{F}^j - \beta^j \tilde{E})$ and $(\alpha \tilde{F}_i^j - \beta^j \tilde{F}_i)$ on cell faces using the HLL approximate Riemann solver (Harten et al. 1983), and a fifth-order WENO reconstruction of E , F_i/E , π_{ij} on cell faces from their cell-centered values (Liu et al. 1994; Jiang & Shu 1996). The time discretization uses an implicit second-order Runge-Kutta method: to evolve the system by a time step Δt , we first take a test step $\Delta t/2$, with the fluxes and explicit source terms computed at the beginning of the time step. We then take a full step Δt , with the fluxes and explicit source terms evaluated from the result of the half step.

To compute the HLL fluxes, we need the characteristic speeds of the system. For the linear system considered here, the minimum and maximum speeds across a face in the direction d are

$$c_\pm = -\beta^d \pm \alpha \sqrt{\pi^{dd}}. \quad (14)$$

Finally, we note that the two-moment scheme is corrected in very optically thick cells (i.e. cells in which $[\kappa_a + \kappa_s] \Delta x \gtrsim 1$, with Δx the grid spacing). Without such a correction, the diffusion of neutrinos in optically thick regions is set by numerical viscosity. This correction effectively transitions between a two-moment scheme and a one-moment scheme, with $F_i(E)$ in optically thick regions set by its known value in the diffusion limit. In practice, we follow the method of Jin & Levermore (1996), whose detailed implementation in the SpEC code is discussed in Foucart et al. (2015). The treatment of high-opacity regions is not modified in our MC-Moment algorithm.

2.3 MC transport

The second and most expensive layer of our transport scheme is a MC algorithm, which we implement in SpEC for this work. Our MC methods are largely inspired from the general relativistic radiation hydrodynamics code *bhlight* (Ryan et al. 2015). We refer the reader to that work for more details on the derivation of a general relativistic MC scheme, and focus here on a summary of the algorithm, as well as on the additional work required to use a MC algorithm to close the moment equations.

In a MC scheme, we evolve *neutrino packets* which sample the distribution function of neutrinos, $f_{(\nu)}$. The ensemble of P packets in the simulation at time t , each representing N_k neutrinos at the spatial coordinates x_k^i and with 4-momentum p_k^μ provides an estimate of the distribution function

$$f_{(\nu)} \sim f_{(\nu),MC} = \sum_{k=0}^P N_k \delta^3(x^i - x_k^i) \delta^3(p_i - p_i^k). \quad (15)$$

We note that the use of lower indices in p_i and upper indices in x^i is required for this equation to be a relativistic invariant. To couple the MC evolution to the moment formalism, we also rely on the MC estimate of the neutrino stress-tensor

$$T_{(\nu),MC}^{\mu\nu} = \sum_{k=0}^P N_k \frac{p_k^\mu p_k^\nu}{\sqrt{\gamma} \alpha p_k^t} \delta^3(x^i - x_k^i). \quad (16)$$

In a MC transport scheme, Boltzmann's equation for $f_{(\nu)}$ can be translated into prescriptions for the creation, annihilation, scattering and propagation of the neutrino packets sampling $f_{(\nu)}$, which we discuss in the following sections. In SpEC, the state of a neutrino packet is entirely determined by its coordinates (t, x^i) , momentum p_i , and neutrino species, as well as the number of neutrinos N_k represented by the packet. As we neglect the masses of neutrinos, the fourth component of the momentum can easily be computed from p_i , e.g. $p^t = \sqrt{\gamma^{ij} p_i p_j} / \alpha$. The spatial components of the coordinates x^i and momentum p_i are evolved in time, while N_k and the neutrino species remain constant during the evolution of a packet. We also regularly need the fluid-frame energy of the neutrinos in the packet

$$\nu = \alpha W p^t - \gamma^{ij} u_i p_j, \quad (17)$$

where $W = \sqrt{1 + \gamma^{ij} u_i u_j}$ is the Lorentz factor of the fluid with respect to an inertial observer.

For high-accuracy evolution of neutrino packets in the MC framework, high-order interpolation of the fluid and metric variables to the position of a neutrino packet would be desirable. However, this would significantly increase the cost of the MC scheme. As limiting the cost of the MC algorithm is our main concern at this point, we make a simpler, less accurate choice: we use cell-centered values of the fluid variables, metric variables, and derivatives of the metric, which are already computed during the evolution of the general relativistic equations of hydrodynamics. We will see in the tests that this is unlikely to be an important contribution to the error budget of our simulations.

2.3.1 Tabulated neutrino-matter interactions

For this code paper, we ignore inelastic scatterings and reactions involving two or more neutrinos. Neutrino-matter interactions are described by a neutrino emissivity $\eta(\rho, T, Y_e, E_{(\nu)})$, absorption opacity $\kappa_a(\rho, T, Y_e, E_{(\nu)})$, and elastic scattering opacity $\kappa_s(\rho, T, Y_e, E_{(\nu)})$, for each species of neutrinos and antineutrinos. The exact interpretation of these variables in the context of a MC algorithm will be discussed in more detail in the following sections.

We use tabulated values of these quantities produced by the open-source NuLib library (O'Connor & Ott 2010), which provides a flexible framework to include a range of neutrino-matter interactions of importance to the merger problem, and let us choose the density of the table in the fluid variables (ρ, T, Y_e) . We use linear interpolation in $[\log(\rho), \log(T), Y_e]$ to interpolate between tabulated values. We discretize the neutrino spectrum into N_E energy bins, with bounds $(E_0 = 0, E_1, \dots, E_{N_E})$. NuLib provides us with values of the opacities at the center of each energy bin. We obtain the opacities at other energies by interpolating linearly in $\log(E_{(\nu)})$. NuLib also provides us with the emissivity per unit volume, integrated over each energy bin. The tabulated values guarantee that η and κ_a satisfy Kirchoff's Law, i.e. that for each energy bin η/κ_a is the energy density of neutrinos in equilibrium with the fluid, integrated over that bin. By enforcing Kirchoff's law in that manner, we make sure that the neutrinos reach the desired equilibrium distribution in optically thick regions. For testing purposes, we also implement an alternative framework in which η, κ_a, κ_s are provided as functions of the spacetime coordinates.

We note that incorporating inelastic scattering of neutrinos by nucleons, electrons, and nuclei into the MC evolution is not particularly complex from an algorithmic point of view, but requires very large tables for the inelastic scattering cross-sections, coupling all energy bins. Neutrino-antineutrino annihilations into e^+e^- pairs are more challenging if one wants to account for the blocking factor of the electrons. Ignoring that factor (which is probably acceptable in the low-density regions where pair annihilation may play an important role), one can define the energy deposition due to pair annihilation from the moments (E, F_i, P_{ij}) for each neutrino species (Fujibayashi et al. 2017), which we already have at our disposal. We plan to incorporate $\nu\bar{\nu}$ annihilations in that approximation, once we begin to use our code to study compact binary mergers.

2.3.2 Emission

To sample the emission of neutrinos, we compute for each cell of volume $\Delta V = \Delta x^1 \Delta x^2 \Delta x^3$ and time interval Δt the number of neutrinos packets N_p emitted with a fluid-frame energy within a given energy bin $[E_{b-1}, E_b]$. Taking advantage of the invariance of the 4-volume $(\sqrt{-g}\Delta V\Delta t)$, and defining $\eta_b(\rho, T, Y_e)$ as the tabulated emissivity per unit volume in that energy bin, we find

$$N_p \approx \sqrt{-g}\Delta V\Delta t \frac{\eta_b(\rho, T, Y_e)}{E_p}, \quad (18)$$

where E_p is the desired energy of each neutrino packet in the fluid frame and $\sqrt{-g} = \alpha\sqrt{\gamma}$. E_p is provided as an input to the code, and effectively sets the number of packets evolved by

the MC algorithm. If $[N_p]$ is the largest integer smaller than N_p , then we create $[N_p]$ neutrinos packets, with a probability $(N_p - [N_p])$ of creating one additional packet.

All packets are created with a fluid-frame neutrino energy $\nu = 0.5 * (E_{b-1} + E_b)$, and represent a number of neutrinos $N_k = E_p/\nu$. The choice to initialize all neutrinos with the energy of the center of the bin was proposed by Richers et al. (2017) and has the advantage to be consistent with the way Kirchoff's law is enforced in the NuLib tables (i.e. by balancing the emissivity η_b integrated over the entire energy bin with the opacity $\kappa_a(\nu)$ at the center of the bin). The time of creation and initial position of the packets are drawn from uniform distributions in (t, x^i) within the volume ΔV and time interval Δt . We note that the choice of uniform sampling in the coordinates x^i could be a significant approximation when using curvilinear coordinates, or if the metric varies significantly over the length of a cell. It may be necessary to use sampling methods which take into account variations in the proper volume element within a cell for applications requiring higher accuracy and/or for non-cartesian grid structures.

The initial direction of propagation of the neutrino packets is drawn so that the packets are isotropically distributed in the fluid frame. The 4-momentum of a neutrino in a given packet is, in comoving coordinates,

$$p^{\mu'} = \nu(1, \sin\theta \cos\phi, \sin\theta \sin\phi, \cos\theta). \quad (19)$$

We draw $\cos(\theta)$ from a uniform distribution in the range $[-1, 1]$ and ϕ from a uniform distribution in the range $[0, 2\pi]$. The 4-momentum of neutrinos in the coordinate frame can then be computed using the orthonormal tetrad described in Sec. 2.1:

$$p^t = \hat{e}^t_{(\lambda')} p^{\lambda'}, \quad (20)$$

$$p_i = g_{i\mu} \hat{e}^{\mu}_{(\lambda')} p^{\lambda'} = \delta_{\kappa'\lambda'} \hat{e}_i^{(\kappa')} p^{\lambda'}. \quad (21)$$

We note that, after that transformation and summing over all bins, the total energy ΔE of the neutrinos created within a cell is, on average and as measured by an inertial observer, $\Delta E = \Delta V\Delta t\sqrt{\gamma}u^t \sum_b \eta_b$. By comparing with the definition of the energy integrated emissivity η used in the evolution of the moments equations, we find that, unsurprisingly, $\eta = \sum_b \eta_b$. The emissivity in the gray two-moment transport can thus be obtained directly from the tabulated emissivities used by the MC algorithm.

2.3.3 Initialization of a cell

The MC algorithm also needs a prescription for the initialization of packets within a cell at the beginning of a time step. Such initialization is required at the beginning of the first time step, as well as in some optically thick regions discussed in Sec. 2.3.5. In optically thick regions, we want these packets to sample the equilibrium distribution of neutrinos. In optically thin regions, we do not have any particularly good guess to rely on, and thus do not create any neutrino packets at the initial time. We assume that the number density of neutrinos on the initial slice within the energy bin $[E_{b-1}, E_b]$ is, in the comoving frame,

$$dn = d^3x^i d\Omega \frac{\eta_b}{\nu[\kappa_a(\rho, T, Y_e, \nu) + a]}, \quad (22)$$

with $\nu = 0.5 * (E_{b-1} + E_b)$. The constant a is semi-arbitrary, and sets the initial energy density of neutrinos in regions of moderate optical depth. At $t = 0$ and for the problems presented here, we choose $a = (\kappa_a + \kappa_s)^{-1} L^{-2}$, where L is a length scale comparable to the typical length scale for variations of $\kappa_{a,s}$. In our tests, we use $L = GM/c^2$, with $M = 1$ (in code units) for idealized tests and $M = M_\odot$ for our test using a core-collapse fluid profile.

A slight complication when sampling the neutrino distribution function on a spatial slice, also discussed in Ryan et al. (2015), is that the 3-volume $\sqrt{\gamma}\Delta V$ is not a relativistic invariant. Accordingly, one has to be careful when sampling in the inertial frame a distribution function which is known only in the frame comoving with the fluid. We can rely on the invariance of $\sqrt{-g}\Delta V p^t$ and the fact that $\sqrt{-g} = 1$ and $p^{t'} = \nu$ in the comoving frame to derive the ratio between the volume element in the comoving frame, $\Delta V' = \Delta x^{1'} \Delta x^{2'} \Delta x^{3'}$, and the volume element in the grid frame, ΔV : $\Delta V' / \Delta V = \sqrt{-g} p^t / \nu$. Using that invariant, we sample the distribution of neutrinos by creating N_p^0 neutrino packets

$$N_p^0 = \sqrt{-g} \Delta V \frac{\eta_b(\rho, T, Y_e)}{E_p [\kappa_a(\rho, T, Y_e, \nu) + a]}. \quad (23)$$

Each packet represents neutrinos with comoving frame energy ν . The non-integer part of N_p^0 is treated as a probability to emit one more packet, the initial position of each packet is drawn from a uniform distribution in ΔV , and the momentum of the neutrinos is drawn from an isotropic distribution in the fluid frame, as for the main emission procedure. Each packet represents $N_k = (E_p / \nu) \times (p^t / \nu)$ neutrinos, and not E_p / ν , to account for the ratio $\Delta V / \Delta V'$.

2.3.4 Propagation, absorption, and scattering

In our code, the evolution of MC packets currently involves three types of operations: the propagation of packets along null geodesics, as well as absorption and scattering of packets sampling neutrino-matter interactions. To evolve a neutrino packet by a time interval Δt , we first determine whether the packet is free-streaming, or whether it is absorbed or scattered by the fluid. Absorption and scattering probabilities can be computed from the infinitesimal optical depth along a geodesic, $d\tau = \kappa \nu d\lambda = (\kappa \nu / p^t) dt$, with $d\lambda$ the increment in the affine parameter ($p^\mu = dx^\mu / d\lambda$). The time interval before the first absorption/scattering is then

$$\Delta t_{s,a} = -\log(r_{s,a}) \frac{p^t}{\kappa_{s,a} \nu}, \quad (24)$$

with $r_{s,a}$ drawn from a uniform distribution in $]0, 1]$. We then determine the smallest of the three time intervals ($\Delta t, \Delta t_a, \Delta t_s$). If Δt is the smallest time interval, the packet is propagated by Δt without interacting with the fluid. If Δt_a is the smallest interval, the packet is propagated by Δt_a and then absorbed (i.e. removed from the simulation). Finally, if Δt_s is the smallest interval, the packet is propagated by Δt_s , then scattered by the fluid. After scattering we begin a new time step with $\Delta t \rightarrow \Delta t - \Delta t_s$. Scattering is performed in the frame comoving with the fluid. As we only consider isotropic elastic scattering, we simply redraw the 4-momentum $p^{\mu'}$ (at constant fluid-frame energy ν), from the same isotropic distribution as during packet creation.

Propagation of a packet along geodesic is performed following the prescription of Hughes et al. (1994),

$$\frac{dx^i}{dt} = \gamma^{ij} \frac{p_j}{p^t} - \beta^i, \quad (25)$$

$$\frac{dp_i}{dt} = -\alpha(\partial_i \alpha) p^t + (\partial_i \beta^k) p_k - \frac{1}{2} (\partial_i \gamma^{jk}) \frac{p_j p_k}{p^t}. \quad (26)$$

We use the same second-order Runge-Kutta time stepping as for the moment algorithm, with the caveat that we use the metric quantities evaluated at the cell center closest to the initial position of the packet. We only switch the cell from which we gather the fluid and metric variables at the end of the time step Δt . This naturally imposes a limit on the timestep $\Delta t \lesssim A \Delta x^i / c_{\max}$, where A reflects our tolerance for how far packets potentially move into a neighboring cell before we use updated values of the metric, and c_{\max} is the maximum grid-coordinate value of the speed of light. In most tests, we choose $A \sim 1/3$, which is comparable to the Courant condition for the evolution of the fluid and of the moments (E, F_i).

2.3.5 Optically thick regions

In theory, we now have at our disposal all of the pieces required for a basic MC scheme: initialization of the simulation, emission of neutrino packets, and interactions with the fluid. We could move on to the computation of the back-reaction on the evolution of the moments. However, this would be prohibitively expensive for at least two reasons. First, the scheme would continuously create and absorb a large number of packets in optically thick regions, where a very small fraction of the emitted packets survive any single time step. Second, in regions in which the scattering opacity $\kappa_s \Delta t \gg 1$, the code would spend too much time propagating neutrino packets over a large number of time intervals $\Delta t_s \ll \Delta t$. Both of these issues can, however, be handled through much cheaper methods.

To do so, we define a 4-dimensional grid in (x^i, ν) , with the spatial discretization being provided by the grid on which we evolve the moments, and the energy discretization provided by the binning used when generating the NuLib table for neutrino-matter interactions. We define three types of cells on this grid. Cells with $\sqrt{\kappa_a(\kappa_a + \kappa_s)} \geq \kappa_{\text{crit}}$ are *optically thick cells*. There, we assume that the neutrinos are in thermal equilibrium with the fluid. Cells which are not optically thick and satisfy $\kappa_s \Delta \tau \geq \tau_{\text{diff}}$ (with $\Delta \tau = \Delta t / u^t$ the proper time of a comoving observer) are called *high-scattering cells*. There, we assume that the diffusion equation is a good approximation to the evolution of the energy density of neutrinos. Finally, cells which are neither optically thick nor high-scattering regions use the standard MC algorithm outlined in the previous sections. The parameters κ_{crit} and τ_{diff} can be specified at run time.

As our algorithm couples the MC evolution to the evolution of the moments, we have a fairly simple solution to the costly evolution of optically thick cells. We simply skip the MC algorithm in optically thick regions, and rely solely on the two-moment scheme in that regime. The two-moment scheme is known to perform well in the diffusion regime, as long as some corrections are applied to the fluxes in order to limit the impact of numerical dissipation. A cell is *masked* if $\sqrt{\kappa_a(\kappa_a + \kappa_s)} \geq \kappa_{\text{crit}}$. Any neutrino packet which

ends a time step in a masked cell is removed from the simulation. When coupling the MC and moment schemes, we assume that neutrinos are in thermal equilibrium with the fluid in masked cells. The proper choice for κ_{crit} depends on the typical length scale over which $\kappa_{a,s}$ vary. We note that we only assume a thermal distribution of neutrinos for the computation of high-order moments and of $\kappa_{a,s}$. The evolution of the moments computes the diffusion of neutrinos through optically thick regions without requiring exact thermal equilibrium.

Entirely neglecting masked cells may create inaccuracies in the evolution of neighboring cells. To provide an effective boundary condition to the MC algorithm, we evolve masked cells which share any boundary with an evolved cell (in 4-dimensional space x^i, ν , and including 1D, 2D, and 3D interfaces), using a modified MC algorithm. All packets which finish a time step in such a boundary cell are removed from the simulation. Packets sampling an equilibrium distribution of neutrinos are redrawn at the beginning of each time step, as during the initialization of the MC scheme (but setting the constant $a = 0$), and the emission of neutrino packets during the time step proceeds as in evolved cells. However, we modify E_p so that no more than N_{max} packets are created in a single energy bin of a single boundary cell. In this paper, we use $N_{\text{max}} = 300$. While destroying and re-creating packets in these cells at each time step may seem highly inefficient, we note that this generally happens in cells in which the number of packets required to sample the equilibrium distribution of neutrinos is comparable to the number of packets created during a time step. The additional use of a strict limit N_{max} on the number of packets created within each of these cells guarantees that our effective boundary conditions does not become an important cost in the MC algorithm.

2.3.6 Approximate treatment of high-scattering regions

In high scattering regions, instead of treating each scattering event individually, we rely on the expected diffusion velocity of packets away from their original location in the comoving frame. Solving the diffusion equation in spherical symmetry, we get that the probability distribution for a packet to move a distance r_d from its original location in the comoving frame is

$$f(\tilde{r}) = \frac{4}{\sqrt{\pi}} \tilde{r}^2 \exp(-\tilde{r}^2), \quad (27)$$

$$\tilde{r} = \sqrt{\frac{3\kappa_s \Delta\tau}{4}} r_d. \quad (28)$$

We could tabulate the function $\tilde{r}(P)$, defined implicitly by

$$\int_0^{\tilde{r}(P)} f(\tilde{r}) d\tilde{r} = P, \quad (29)$$

and then randomly draw P from a uniform distribution to obtain $r_d(P)$. In fact, we find that we can obtain a better approximation of the diffusion limit for moderate values of $\kappa_s \Delta\tau$ if we set

$$\int_0^{\tilde{r}(P)} f(\tilde{r}) d\tilde{r} = P \frac{\int_0^{\sqrt{3\kappa_s \Delta\tau/4} \Delta\tau} f(\tilde{r}) d\tilde{r}}{1 - \exp(-\kappa_s \Delta\tau)}, \quad (30)$$

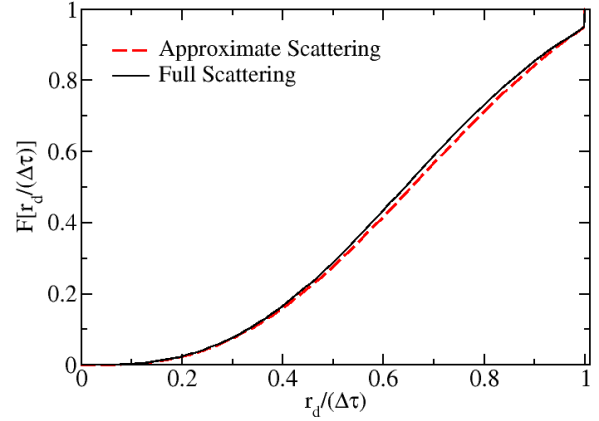


Figure 1. Distribution function of $r_d/(\Delta\tau)$, the ratio of the distance covered by a packet to the elapsed proper time, for $\kappa_s \Delta\tau = 3$. We show the approximate distribution function used in our code, and the results of scattering experiments in which 10^8 MC packets are propagated with scatterings properly treated as individual events. Even for $\kappa_s \Delta\tau = 3$, the agreement between the exact and approximate treatment is quite good (and it only improves with increasing optical depth).

and set $r_d = \Delta\tau$ whenever that formula predicts $r_d > \Delta\tau$, to avoid violating causality. Cases in which $r_d > \Delta\tau$ are interpreted as packets which do not experience any scattering interactions. Eq. 30 is obtained by renormalizing Eq. 29, using the constraint that the probability for a packet to avoid any scattering (i.e. to get $r_d > \Delta\tau$) is $\exp(-\kappa_s \Delta\tau)$. With that normalization, we find good agreement between the approximate distribution of r_d and the distribution obtained by treating scattering events individually, for optical depths as low as $\kappa_s \Delta\tau \sim 3$ (see Fig. 1).

In practice, when evolving a neutrino packet, we always evolve the packet exactly up to its first interaction. If that interaction is a scattering event, and the remaining time in the time step is such that $\kappa_s \Delta\tau > \tau_{\text{diff}}$, we continue the time step using the diffusion approximation. We then draw a new absorption time Δt_a and evolve the packet by $\Delta t = \min(\Delta t, \Delta t_a)$ as follows. We randomly draw P from a uniform distribution in $]0, 1]$ to obtain $f_{\text{free}} = r_d/\Delta\tau$. We transport the neutrino packet with the fluid for a proper time $\Delta\tau_{\text{fl}} = (1 - f_{\text{free}})\Delta\tau$, and then propagate the packet for a proper time $\Delta\tau_{\text{free}} = f_{\text{free}}\Delta\tau$ in a random direction drawn from an isotropic distribution in the comoving frame. If the packet is absorbed, we then remove it from the simulation.

The advection of a packet by the fluid proceeds as follows. We define a momentum $p^\mu = At^\mu + Bu^\mu$, setting A and B by requiring that $p^\mu p_\mu = 0$ and $p^\mu u_\mu = -v$. Then we propagate the packet along the null geodesic defined by p^μ for a

time $\Delta t' = \Delta t_{\text{fl}}(u^i p^i)/(u^t p^t)$. Practically,

$$\frac{A}{B} = -\frac{u_t + \sqrt{u_t^2 + g_{tt}}}{g_{tt}}, \quad (31)$$

$$B = \frac{\nu}{1 - \frac{A}{B}u_t}, \quad (32)$$

$$\frac{u^i p^i}{u^t p^t} = \frac{A + Bu^t}{Bu^t}. \quad (33)$$

As these equations are singular for a fluid with $u^i = 0$, we only go through this procedure when $\delta_{ij}u^i u^j \geq 10^{-10}$. Otherwise, advection with the fluid motion simply keeps a packet at its current location. This algorithm does not exactly reproduce the diffusion of a packet in curved spacetime, but guarantees that packets experience the proper gravitational redshift, and are advected by the fluid. The choice to evolve along a null geodesic instead of along u^μ is done so that we can evolve the momentum of the packet according to Eq. 26, which assumes $p^\mu p_\mu = 0$. We then propagate the packet for $\Delta t_{\text{fl}} - \Delta t'$ along t^μ . The vector t^μ is timelike, not null, but we make the approximation that the 4-momentum of neutrinos in the packet is constant during that step.

We then randomly draw a direction of propagation from an isotropic distribution in the fluid frame, as when emitting new packets, keeping the fluid frame energy ν constant. This generates a new fluid frame momentum for the packet, p_{free}^μ . There is now a subtlety in the determination of the time interval over which we let the packet free stream in the direction of p_{free}^μ . It is not simply $\Delta t_{\text{free}} = f_{\text{free}}\Delta t$, because packets propagating in different directions should be propagated for the same time interval *in the fluid frame*. The correct time step for the free propagation of a packet is $\Delta t_{\text{free}} = f_{\text{free}}\Delta t[p^t/(vu^t)]$. With this weighting of the time step, the average propagation velocity of freely propagating packets is u^i/u^t , as desired. It is worth noting that because of this weighting, a given packet may be propagated to a time larger or smaller than initially requested. In our MC algorithm, there is however no particular requirement for the propagation of all packets to end at the same time in any given call to the MC algorithm, so this does not create any issue.

The last step in our approximate treatment of regions of high κ_s is the most complex. Once a packet has been propagated, we need to determine what its momentum will be at the beginning of the next time step. We define the angles (θ_2, ϕ_2) determining the orientation of that momentum vector in the fluid frame, in a spherical polar coordinate system whose polar axis is the momentum p_{free}^μ . The momentum at the beginning of the next time step is then, in the fluid frame,

$$\begin{aligned} p^{0'} &= \nu \\ p^{1'} &= \nu(-\sin\theta_2 \cos\phi_2 \cos\theta \cos\phi + \sin\theta_2 \sin\phi_2 \sin\theta \\ &\quad + \cos\theta_2 \sin\theta \cos\phi), \\ p^{2'} &= \nu(-\sin\theta_2 \cos\phi_2 \cos\theta \sin\phi - \sin\theta_2 \sin\phi_2 \cos\phi \\ &\quad + \cos\theta_2 \sin\theta \sin\phi), \\ p^{3'} &= \nu(\sin\theta_2 \cos\phi_2 \sin\theta + \cos\theta_2 \cos\theta). \end{aligned}$$

By symmetry, we can always draw ϕ_2 from a uniform distribution in $[0, 2\pi[$. The simplest options for θ_2 would be to either draw $\cos\theta_2$ from an isotropic distribution in $[-1, 1]$,

which effectively means that the $p^{\mu'}$ will be isotropically distributed in the fluid frame, or to set $\theta_2 = 0$ and use the average direction of propagation of the packets away from the motion of the fluid as their final direction of propagation. We will see that either option fails to reproduce solutions obtained without using any approximation in regions of high κ_s . By inspection of three sets of scattering experiments in which we scattered $\sim 10^8$ packets through optical depths $\kappa_s = (3, 10, 30)$, however, we find that to high accuracy the distribution of θ_2 only depends on the ratio $f_{\text{free}} = \Delta\tau_{\text{free}}/\Delta\tau$. Furthermore, a good fit to the results of these experiments can be obtained by setting

$$\cos\theta_2 = B(f_{\text{free}}) - [1 + B(f_{\text{free}})] \exp\left[r \ln\left(\frac{B(f_{\text{free}}) - 1}{B(f_{\text{free}}) + 1}\right)\right]. \quad (34)$$

To capture the fact that $p^{\mu'}$ should be isotropic for $f_{\text{free}} = 0$ and that $\theta_2 = 0$ for $f_{\text{free}} = 1$, we want $B(0) \rightarrow \infty$ and $B(1) \rightarrow 1$. In practice, we fit B to match our scattering experiments, and tabulate the result of those fits. We then interpolate B linearly in f_{free} . We use $B_i = B(0.05i)$ with

$$\begin{aligned} B_i = & (1000, 18.74, 7.52, 4.75, 3.51, 2.78, 2.32, 2.00, \\ & 1.77, 1.60, 1.47, 1.36, 1.28, 1.21, 1.15, 1.10, \\ & 1.07, 1.04, 1.019, 1.0027, 1.0000001) \end{aligned} \quad (35)$$

and $i = 0, 1, \dots, 20$. This approximation is tested in Sec. 3.4, and shows very good agreement with a full treatment of individual scatterings.

2.4 MC-Moments Coupling

The role of the MC evolution in our algorithm is to provide missing information about the distribution function of neutrinos to the evolution of the moments. In particular, we have shown in Sec. 2.2 that the moment scheme needs the Eddington tensor $\pi_{ij} = P_{ij}/E$, and the energy-averaged absorption and scattering opacities $\kappa_{a,s}$. In order to compute the evolution of the electron fraction of the fluid, we also need the number emission and absorption opacity, η_N and κ_N . Indeed, the evolution equation for the composition of the fluid is

$$\partial_\mu(\rho Y_e \sqrt{-g} u^\mu) = - \sum_i \text{sign}(v_i) \sqrt{-g} (\eta_N - \kappa_N J), \quad (36)$$

where the sum is taken over all neutrino species, and $\text{sign}(v_i)$ is 1 for ν_e , -1 for $\bar{\nu}_e$, and 0 for heavy-lepton (anti)neutrinos.

We have already seen that the emissivity is simply $\eta = \sum_b \eta_b$, with η_b the integrated emissivity within an energy bin. Similarly, $\eta_N = \sum_b 2\eta_b/(E_{b-1} + E_b)$. The other quantities will be derived from ratios of the MC moments E_{MC} , $F_{i,MC}$, $P_{ij,MC}$, J_{MC} , $(\kappa_a J)_{MC}$, $(\kappa_s J)_{MC}$, and $(\kappa_N J)_{MC}$. All of these moments are computed following the same strategy. Any MC moments X_{MC} is divided into three contributions

$$X_{MC} = X_{thick} + X_{prop} + X_{comov}. \quad (37)$$

X_{thick} is the contribution from high opacity cells, where we assume that neutrinos are in equilibrium with the fluid. X_{free} is the contribution from free-streaming packets. X_{comov} the contribution from packets advected with the fluid in high-scattering regions. Each of these components rely on a different estimate of the stress-energy tensor.

For X_{thick} , each energy bin which is not evolved by the MC algorithm is assumed to contribute

$$T_{thick}^{\mu\nu} = \frac{\eta_b}{\kappa_{a,b}} \left(\frac{4u^\mu u^\nu + g^{\mu\nu}}{3} \right), \quad (38)$$

as appropriate for neutrinos in equilibrium with the fluid. For each propagating packet, we have

$$T_{free}^{\mu\nu} = N_k \frac{p_k^\mu p_k^\nu}{\sqrt{\gamma} \alpha p_k^t} \delta^3(x^i - x_k^i), \quad (39)$$

while for packets comoving with the fluid, we use the approximation

$$T_{comov}^{\mu\nu} \sim N_k \frac{v^2}{(vu^t)} \left(\frac{4u^\mu u^\nu + g^{\mu\nu}}{3\alpha\sqrt{\gamma}} \right) \delta^3(x^i - x_k^i), \quad (40)$$

which assumes an isotropic distribution of momenta in the comoving frame. The full moment is then obtained by integrating over the proper volume $\sqrt{-g}\Delta V\Delta t$ of the cell (for the optically thick limit), or the propagating time Δt of a packet. For example, for the energy density E_{MC} ,

$$\begin{aligned} E_{MC} &= \sum_{b,thick} \sqrt{-g}\Delta V\Delta t \frac{\eta_b}{\kappa_{a,b}} \left(\frac{4W^2 - 1}{3} \right) \\ &+ \sum_{k,free} N_k (\alpha p_k^t)^2 \frac{\Delta t}{p_k^t} \\ &+ \sum_{k,comov} N_k v \left(\frac{4W^2 - 1}{3} \right) \frac{\Delta t}{u^t}. \end{aligned} \quad (41)$$

The first sum is taken over the energy bins in which the cell is assumed to be optically thick, while the other two are taken over the paths of packets either propagating along null geodesics or comoving with the fluid. We note that there are several abuses of notation in the previous formula. A single packet undergoing scattering interactions may contribute to both the free-streaming and comoving component of the stress-energy tensor during a single time step, with different Δt , and may contribute multiple time to the free-streaming component of the stress-energy tensor with different Δt and p^μ . Practically, the calculation is performed by letting each packet contribute to the computation of the moments whenever it is evolved in time. The optically thick regions are taken into account during the emission step, when we determine which cells do not need to be evolved using the MC algorithm.

The other moments can be obtained by taking different projections of the stress tensor, except for $(\kappa_N J)_{MC}$ which is

$$\begin{aligned} (\kappa_N J)_{MC} &= \sum_{b,thick} \sqrt{-g}\Delta V\Delta t \frac{\eta_b}{v} \\ &+ \sum_{k,free} N_k \kappa_a v \frac{\Delta t}{p_k^t} + \sum_{k,comov} N_k \kappa_a \frac{\Delta t}{u^t}. \end{aligned} \quad (42)$$

With these moments at hand, we can compute $\pi_{ij} = P_{ij,MC}/E_{MC}$, and $\kappa_{a,s,N} = (\kappa_{a,s,N} J)_{MC}/J_{MC}$. We also define the average number of packets per cell (multiplied by the proper time interval spent in that cell) N_{MC} as

$$\begin{aligned} N_{MC} &= \sum_{b,thick} \sqrt{-g}\Delta V\Delta t \frac{\eta_b}{\kappa_a E_p} \\ &+ \sum_{k,free} \frac{v\Delta t}{p_k^t} + \sum_{k,comov} \frac{\Delta t}{u^t}. \end{aligned} \quad (43)$$

To time-average the MC moments over multiple time steps, and thus allow us to use a lower number of packets in the simulation, we continuously add to all of the above moments. Instead of resetting the moments to zero at the beginning of a time step, we multiply all moments (including N_{MC}) using

$$X_{MC} = X_{MC}^0 \min \left[\exp \left(-\frac{\Delta t}{u^t \tau_d} \right), \frac{N_0 \Delta x_{avg}}{N_{MC}} \right]. \quad (44)$$

Thus, τ_d is a minimum damping timescale in the comoving frame, while N_0 is the desired number of packets over which we average the neutrino distribution function, assuming that we can accumulate N_0 packets over a timescale shorter than τ_d . The distance $\Delta x_{avg} = (\sqrt{\gamma}\Delta x^1 \Delta x^2 \Delta x^3)^{1/3}$ provides a rough estimate of the propagation time across a cell. A large N_0 implies small statistical errors in the MC moments, but longer averaging timescales. Unless otherwise specified, we use $N_0 = 100$, which should lead to $\sim 10\%$ relative errors in the MC moments. The actual accuracy of the method will however be better than this in optically thick regions, where more than 100 packets live in a cell at any given time.

We also need a backup prescription for the computation of the moments when the MC algorithm does not have enough packets to provide any reliable information. Whenever we have a cell with $N_{MC} < N_{min}\Delta x_{avg}$, all opacities are set to zero and the Eddington tensor is computed using the M1 closure, $\pi_{ij,M1}$. During the moment evolution, we also use $\pi_{ij,M1}$ at cell faces if both neighboring cells have $N_{MC} < N_{min}\Delta x_{avg}$. When that is the case, the characteristic speeds of the system are estimated assuming the nonlinear M1 closure. In this work, we use $N_{min} = 5$.

Finally, we will show in the code tests that, at finite resolution, the moment and MC algorithms can diverge, leading to a meaningless Eddington tensor when π_{ij} is computed from the MC evolution, and to numerical instabilities. To avoid this issue, we define a deviation between the MC and moment algorithms as

$$(\delta F)^2 = \gamma^{ij} \left(\frac{F_{i,MC}}{E_{MC}} - \frac{F_i}{E} \right) \left(\frac{F_{j,MC}}{E_{MC}} - \frac{F_j}{E} \right), \quad (45)$$

$$\epsilon = 0.5 \left[1 + \operatorname{atan} \left(\frac{\min(\delta F, 1) - 0.5}{0.1} \right) \right]. \quad (46)$$

The Eddington tensor is then defined as

$$\pi_{ij} = \epsilon \pi_{ij,M1} + (1 - \epsilon) \pi_{ij,MC}. \quad (47)$$

This introduces a slight additional lag in the reaction of the evolution equations to a change in the closure, but also provides additional stability. The approximate characteristic speeds are similarly corrected as $c_\pm = \epsilon c_\pm^{MC} \pm (1 - \epsilon) c_\pm^{M1}$ with c^{M1} the largest characteristic speed (in absolute value) for the evolution of the moments, assuming the M1 closure. Potential alternatives to this prescription includes promoting $\delta F_i = \left(\frac{F_{i,MC}}{E_{MC}} - \frac{F_i}{E} \right)$ to an evolved variable, and using constraint damping to drive that variable to zero, or using high-order/low-order methods in which δF_i is used to compute a stabilizing source term in the evolution equations for F_i . We do not investigate these other methods in this work.

2.5 Fully coupled general relativistic radiation hydrodynamics

Although in this work we never evolve Einstein’s equations nor the general relativistic equations of hydrodynamics, our MC-Moments algorithm is already fully integrated into SpEC. The coupled general relativistic radiation hydrodynamics system is put together as follow. Einstein’s equations and the general relativistic equations of hydrodynamics are evolved as usual in SpEC, using a third-order Runge-Kutta time stepping method. Einstein’s equations are evolved on a pseudospectral grid, and the general relativistic equations of hydrodynamics on a finite volume grid (see [Duez et al. 2008](#); [Foucart et al. 2013](#)). The source terms are communicated between these grids at the end of each full step of the Runge-Kutta algorithm. Values at intermediate steps are obtained by first-order extrapolation in time. The neutrinos are treated using operator splitting. At the end of a metric/fluid time step Δt , we evolve the two-moments equations by Δt . During the neutrino timestep, we also modify the fluid variables to take into account the impact of neutrino-matter interactions on the energy density, momentum, and composition of the fluid.

The MC algorithm can, in theory, be called at arbitrary time intervals. In particular, if the averaging timescale is long compared to Δt , there is a priori no need to call the MC evolution at each timestep. However, the main cost of the MC evolution is the propagation of neutrino packets, and neutrino packets propagate at the speed of light between neighboring cells. We argued in [Sec. 2.3.4](#) that this leads to a limit on the time step comparable to the Courant condition limiting the time step for the evolution of the fluid and moments of $f_{(\nu)}$. Accordingly, there is very little to gain by using a different timestep for the fluid evolution and for the MC algorithm. One exception is if the pseudospectral grid used to evolve the metric is much finer than the finite volume grid used for the fluid/neutrinos, and sets the timestep for the fluid/metric evolution. In that case, it may be beneficial to only call the MC algorithm every n steps of the metric/fluid evolution, with n chosen so that $n\Delta t \lesssim \Delta x/3$. As the code tests below do not evolve Einstein’s equations, we do not encounter such a case here, and set $n = 1$.

Each step of the MC algorithm proceeds, in our current implementation, as follow:

- Packets are created as described in [Secs. 2.3.2](#) and [2.3.5](#), as needed to represent neutrino emission and the sampling of an equilibrium distribution of neutrinos in optically thick cells at the boundary of the MC domain. Each packet is initially owned by the processor which owns the fluid cell in which the packet is created. In optically thick cells which are not evolved with the MC algorithm, we add to the MC moments the contribution of neutrinos in thermal equilibrium with the fluid.

- Packets are propagated, scattered, and absorbed following the methods of [Secs. 2.3.4](#) or [2.3.6](#). The contribution to the MC moments of each packet is computed at this time.

- The MC moments are communicated to the ghost zones of the fluid grid, so that the evolution of the moments can use values of the MC moments in ghost zones.²

- All packets which ended their evolution in a ghost zone of the fluid grid are transferred to the processor which evolves the region of the grid corresponding to that ghost zone.

The parallelization method chosen here, in which packets are simply owned by the processor which also owns the fluid cell in which the packets reside, is highly suboptimal. Indeed, the distribution of packets across grid cells is very uneven, with most packets residing in the most optically thick cells evolved by the MC algorithm. We expect that, for efficient 3D evolution of neutron star mergers, a more advanced parallelization scheme will be necessary. In this work, however, we focus solely on the stability and accuracy of the mixed MC-Moments algorithm, and do not attempt to implement a more advanced parallelization scheme.

We also note that the methods described here are mostly useful for systems in which we can rely on time-averaged moments to reduce the cost of the simulation. This makes their application to neutron star merger simulations very promising, but their use in radiatively dominated accretion disks more uncertain. In accretion disks, we may have optically thin regions in which the cooling time scale is shorter than the evolution time step, and radiatively dominated regions in which small errors in the neutrino pressure can create large errors in the fluid evolution. The savings provided by time-averaging the moments may be negligible in those regimes. A potential alternative would be to incorporate in our scheme implicit MC techniques, as developed by [Roth & Kasen \(2015\)](#) – although how this would interface with the rest of our algorithm is highly speculative at this point.

3 CODE TESTS

3.1 Packet propagation

As a first code test, we consider the propagation of a single neutrino packet in curved spacetime. This allows us to verify that free-streaming packets follow null geodesics, and to obtain an estimate of the numerical error due to the use of low-order methods for packet propagation along geodesics. We consider a non-spinning black hole of mass $M_{\text{BH}} = 1$, and use the Kerr-Schild metric $g_{\mu\nu} = \eta_{\mu\nu} + 2l_{\mu}l_{\nu}/r$, with $l_{\mu} = (1, x_i/r)$. The packet is initialized at $x^i = (0, 4, 0)$, with a fluid-frame energy $\nu = 1$ and 4-momentum set by the additional requirements that $p^2 = p^3 = 0$. We follow the packet up to the point at which $x^2 = 0$. We show the error in the location of the packet as a function of the azimuthal angle $\phi = \text{atan}(x^1/x^2)$, for grid spacings $\Delta x = (1/6, 1/9, 1/12)$ and time steps $\Delta t = (0.075, 0.05, 0.0375)$. This is a relatively low resolution compared to what is typically used in simulations of NSNS and NSBH mergers. Yet, we see on [Fig. 2](#) that even

by a given processors. They are not evolved, but they are needed for high-order interpolation from cell centers to cell faces. For the fifth-order WENO reconstruction used here, we need 3 buffer cells along each dimension. The value of the fields in those cells have to be overwritten by their value on the processor in which that region of the grid is actually evolved.

² Ghost zones are buffer grid cells neighboring the cells evolved

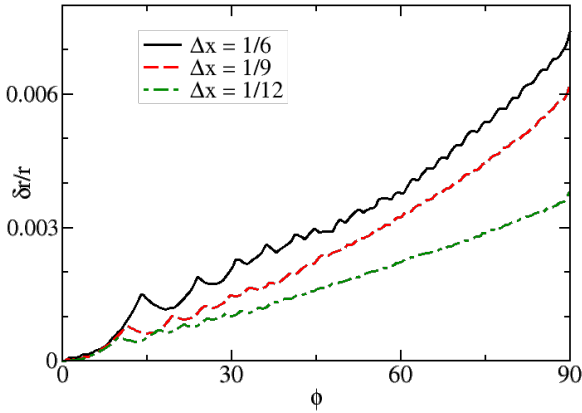


Figure 2. Numerical error in the propagation of a single packet around a unit mass black hole. The packet is initialized at $x^i = (0, 4, 0)$, with a momentum such that the packet initially propagates along the $+x$ direction. While the low-order methods used to propagate packets cause slow convergence of the solution, the amplitude of the numerical error is quite small.

for a packet initialized fairly close to the black hole, the numerical error remains small, $\lesssim 0.5\%$. Similar errors are observed for the conserved energy and angular momentum of the packets, p_t and p_ϕ . We thus conclude that the low-order propagation methods used in this work are unlikely to be a significant source of error in merger simulations.

The convergence of the numerical solution to the expected analytical trajectory is quite slow. In fact, formal convergence is only observed at very early times, for $\phi \lesssim 5^\circ$. This indicates that to obtain reliable error estimates for the propagation of neutrino packets, higher order methods would be required. However, as the actual error in the evolution of the packets observed here is negligible compared to other sources of error in current general relativistic radiation hydrodynamics simulations, we do not consider it worthwhile to go beyond the cheap, low-order methods implemented in our current code.

3.2 Single Beam in Curved Spacetime

We now move to the coupled MC-Moments scheme, with a similar setup. Instead of emitting a single packet at $x^i = (0, 4, 0)$, we create packets in a small sphere of radius $r_s = 0.2$ around that point. All packets are still initialized with a momentum such that $p^2 = p^3 = 0$, $\nu = 1$. The emissivity is set to 10^6 packets per unit volume (with $G = c = 1$). With the grid spacing $\Delta x = 0.057$ and time step $\Delta t = 0.025$ used in our simulation, this corresponds to only ~ 4.6 packets per time step in each cell within the emitting region. Consistent source terms are provided to the evolution of the moments. This setup allows us to test two important aspects of the code: the evolution of a single beam in curved spacetime, and the collapse of that beam into the $x^3 = 0$ plane as it crosses the $x^2 = 0$ plane (as all packets emitted with $p^2 = p^3 = 0$ on the $x^1 = x^3 = 0$ axis pass through the $x^2 = x^3 = 0$ axis).

A volume rendering of the beam is shown on Fig. 3.

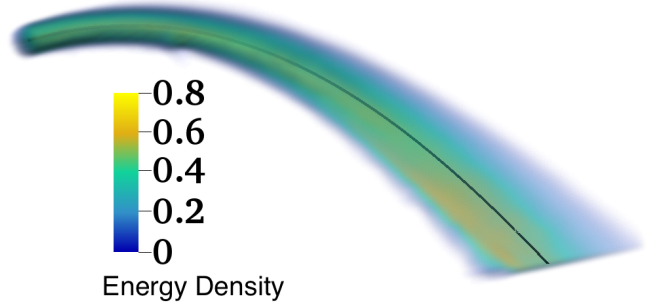


Figure 3. Beam distorted by the gravitational potential of a non-spinning black hole of unit mass. All neutrinos are emitted from a small sphere of radius $r_s = 0.2$ around $x_c = (0, 4, 0)$, with initial motion parallel to the X-axis (top left part of the plot). With that choice, all neutrinos pass through the $(x^2 = 0, x^3 = 0)$ line (bottom right part of the plot). At that point, the height of the beam goes down to a single grid cell. The solid black lines is the analytical result for the null geodesic at the center of the beam. The color scale shows the neutrino energy density E .

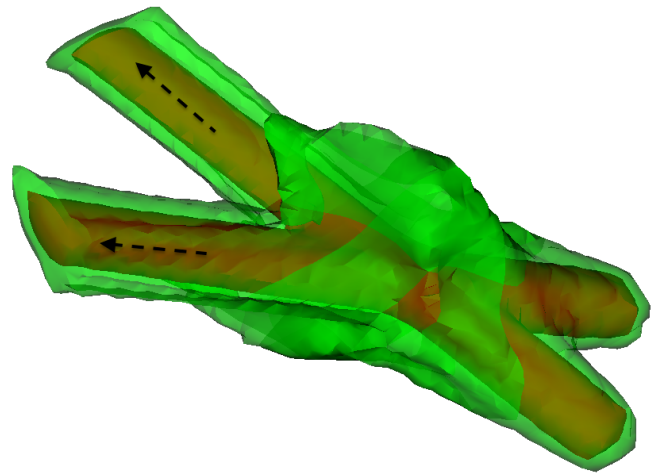


Figure 4. Two beams of neutrinos emitted from spheres of radii $r_s = 0.3$ and centers $c_1 = (-2, -1, 0)$, $c_2 = (-1, -2, 0)$, towards the origin. We show contours at 10% and 1% of the maximum energy density E .

We see that the beam follows the expected null geodesic, and that the height of the beam becomes of the order of Δx on the $x^2 = x^3 = 0$ line. This does not happen when using the M1 closure for the evolution of the moments: with that closure, a convergent beam is partially supported by unphysical radiation pressure, and the evolution of the beam converges to an erroneous solution. With the MC closure, we can collapse the beam to a height of a single grid cell!

3.3 Crossing Beams

For our next test, we consider a well-known problem for which the standard M1 closure fails spectacularly. We set up

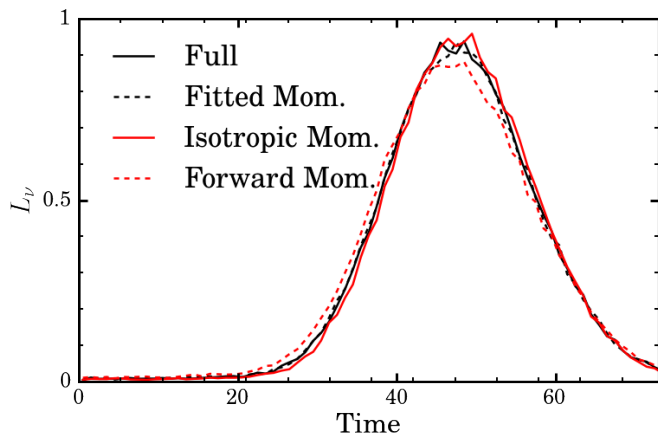


Figure 5. Luminosity of the MC packets leaving the computational domain, as a function of time, for a Gaussian pulse advected in a moving medium. The medium has $\kappa_a = 0$ and $\kappa_s = 100$, with $\Delta t = 0.05$, so that the code can use the simplified evolution of neutrino packets in high- κ_s regions. The different curves represent results without using the approximate method (Full), with our preferred approximate method in which the final momenta are fitted to the results of scattering experiments (Fitted Mom.), and with momenta chosen either isotropically in the fluid frame (Isotropic Mom.) or always in the direction of propagation of the packet away from the fluid motion (Forward Mom.). The latter is the only method which doesn’t quite reproduce the correct luminosity.

two coplanar beams of neutrinos, emitted from two spheres of radii $r_s = 0.3$ and centers $c_1 = (-2, -1, 0)$, $c_2 = (-1, -2, 0)$. The beams are emitted towards the origin, and cross each other there. With the M1 closure, the beams collide and then propagate along the direction of their average momentum (see e.g. Foucart et al. 2015) – a more obvious manifestation of the problems encountered by the M1 closure for converging beams, already mentioned in the previous section.

With the MC closure, on the other hand, the beams properly cross, as shown in Fig. 4. Due to the use of time-averaged moments, and the finite time required for the moment evolution to react to the passage of packets in the MC evolution, our evolution is not entirely free of artifacts: numerical diffusion at the level of a few percents of the maximum density of the beams is clearly visible in Fig. 4. Yet, in this test, the time-averaged MC closure provides results which are far superior to the M1 closure.

3.4 Diffusion through a region of high scattering opacity

One of the most complex part of our coupled MC-Moments algorithm is the approximate treatment of regions of high scattering opacities, discussed in Sec. 2.3.6. A standard test for radiation transport in optically thick regions is the advection of a Gaussian pulse in a fluid with constant velocity $u^\mu = W(1, v, 0, 0)$, on a Minkowski background and with opacities $\kappa_a = 0$, $\kappa_s \Delta x \gg 1$. In our case, this is however a fairly trivial test: the evolution of the moments is already corrected to reproduce the diffusion limit when $(\kappa_s + \kappa_a) \Delta x \gg 1$, and does not use the MC closure in that regime. While our code

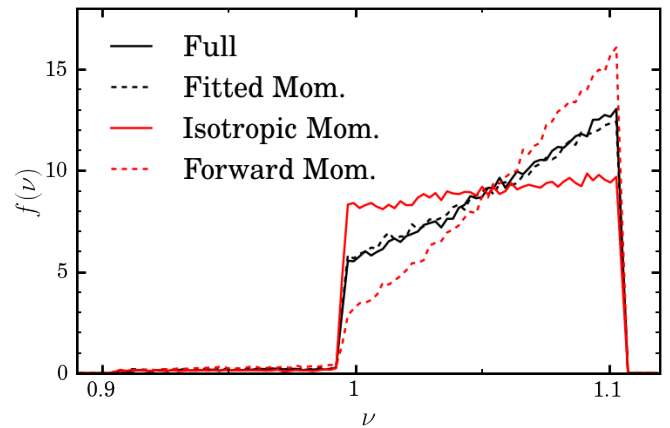


Figure 6. Spectra of the MC packets for the same test as in Fig. 5. We see that the various approximate methods to choose the final momenta of neutrino packets in our approximate treatment of scattering events now lead to significant differences in the spectra, with only the method in which the final momenta are fitted to the results of scattering experiments providing a good match to the correct solution.

does maintain a steady pulse profile comoving with the fluid, as expected, this is not a particularly useful test of our algorithm. We simply note that the main source of error in this test comes from the reconstruction of the moments on cell faces. That error is negligible when using the high-order WENO5 reconstruction in the evolution of the moments, but can be significant for more dissipative reconstruction methods.

A more interesting test of our algorithm is when $\kappa_s \Delta t \gtrsim 3$: in that case, the evolution of the moments uses a weighted average of the MC closure and of the diffusion approximation and, more interestingly, the MC algorithm uses the complex method approximating the propagation of neutrino packets through a region of large κ_s described in Sec. 2.3.6.

To test this regime, we consider a simple cartesian grid with spacing $\Delta x = 0.2$, and initialize a Gaussian pulse of width $\Delta = 0.5$ at the origin. The background fluid has a velocity $u^\mu = W(1, 0.1, 0, 0)$ and an energy-independent $\kappa_s = 100$ (except within 3 cells of the boundary, where $\kappa_s = 0$). We use a time step $\Delta t = 0.05$. We find that the advection and diffusion of the pulse is well captured, fairly independently of the details of the algorithm used for regions of high κ_s . This is most likely because the evolution of the moments still relies largely on the diffusion limit for $\kappa_s \Delta x = 20 \gg 1$. On the other hand, we find that using a well-calibrated prescription for the choice of the momentum of the neutrino packets at the end of their approximate propagation through high κ_s regions plays an important role in properly capturing the spectrum of the neutrinos escaping that region.

Fig. 5 shows the flux of MC packets across the domain boundary as a function of time for 4 different evolutions: one in which scattering events are treated individually, which should be an accurate representation of the true solution, one using our favored prescription for setting the momentum of packets at the end of a time step in which we make use of our approximate algorithm for the propagation of packets through a high- κ_s region (“Fitted” momenta, see Sec. 2.3.6),

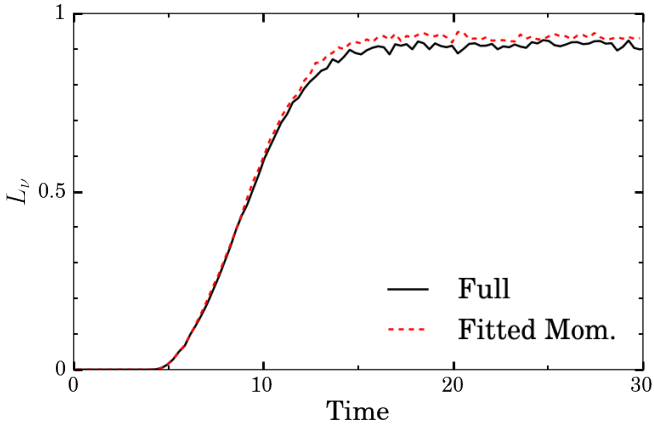


Figure 7. Same as Fig. 5, but for a spherical shell $2.5 < r < 5$ with $\eta = 1$, $\kappa_a = 1$, and $\kappa_s = 100$ around a non-spinning BH. We only show our preferred method for the determination of the momentum of packets, and the result of an evolution without using any approximation in high-scattering regions. The luminosity is normalized for ease of visualization. The approximate method overestimates the luminosity by $\sim 2\%$.

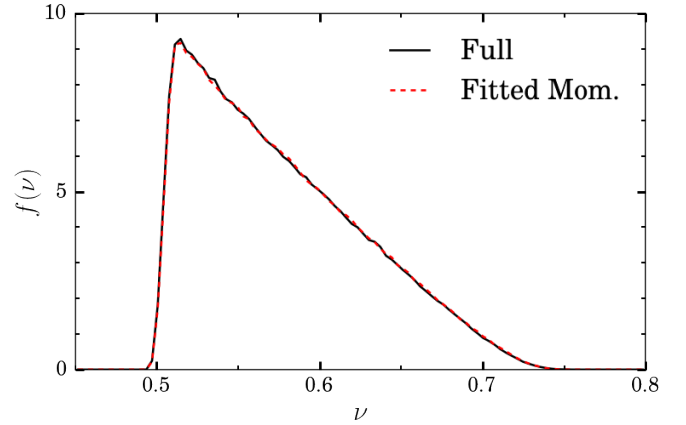


Figure 8. Same as Fig. 6, but for a spherical shell $2.5 < r < 5$ with $\eta = 1$, $\kappa_a = 1$, and $\kappa_s = 100$ around a non-spinning BH. We only show our preferred method for the determination of the momentum of packets, and the result of an evolution without using any approximation in high-scattering regions. Both methods return very similar spectra.

one using an isotropic distribution in the fluid frame for those momenta (“Isotropic” momenta), and one in which these momenta are set along the average direction of propagation of the packets away from the motion of the fluid. We see that only the latter method shows a (small) error in the flux of neutrino packets. All methods also agree well with the measured flux in the evolution of the moments.

Fig. 6 shows the spectrum of the packets leaving the grid. Now, only the “Fitted” method properly matches the evolution in which we do not use any approximation in high- κ_s regions. Large errors in the energy spectrum of the neutrinos leaving a high- κ_s region could have a significant impact on the absorption of neutrinos in lower-density regions in simulations where $\kappa_{a,s}$ is energy dependent. Accordingly, we consider it worthwhile to use the more complex (but not significantly more expensive) method derived in Sec. 2.3.6 to evolve neutrino packets in high- κ_s regions.

As a more demanding test of our approximate method, we now consider a shell $2.5 < r < 5$ with $\kappa_s = 100$, $\eta = 1$, and $\kappa_a = 1$, set around a non-spinning black hole of unit mass. We perform the simulation in octant symmetry, with a box of length $L_{\text{box}} = 7$, a grid spacing $\Delta x \sim 0.13$, and a time step $\Delta t = 0.05$. The fluid is considered to be at rest with respect to an inertial observer, and thus has a non-zero infall velocity in the grid frame. Accordingly, this test involves non-zero fluid velocity, and a non-trivial metric. It tests, among other things, that our approximate method properly captures the gravitational redshift of the diffusing packets. Figs. 7-8 again show the flux and energy spectrum of packets escaping the domain. We see very good agreement in the spectrum between the full treatment of scatterings and the approximate method, and errors of $\sim 2\%$ in the number of packets leaving the grid. For such a complex setup, we consider this to be an acceptable error at this point.

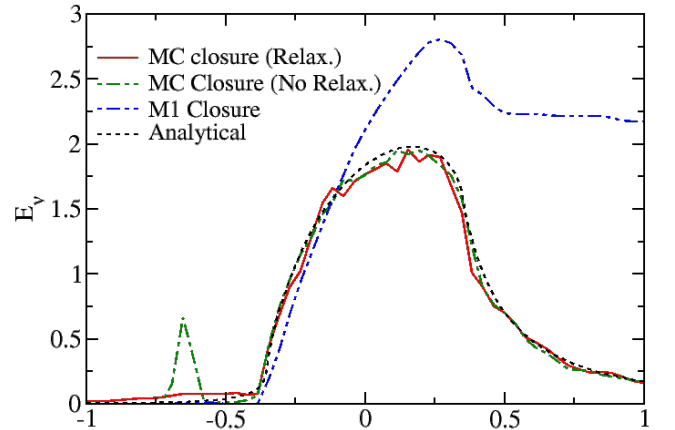


Figure 9. Energy density of neutrinos around an emitting sphere of radius $r_s = 0.5$ with a Lorentz factor $W = \sqrt{2}$, shown along the axis parallel to the direction of propagation of the sphere and passing through its center. The dashed black curve shows the known analytical solution for this problem. The dot-dashed blue curve is for the moment formalism with M1 closure. The effect of the radiation shock created by converging neutrinos along the direction of propagation of the sphere is clearly visible in the $x > 0$ region. The green dot-dashed curve shows an evolution with the MC-Moment scheme in which we use directly the Eddington tensor computed from the MC evolution. While better than the M1 closure within and in front of the sphere, a numerical artifact due to the accumulation of energy in a region in which zero-speed modes exist is visible downstream of the emitting sphere. Finally, once we use a weighted average of the MC and M1 closures, we obtain the thick red line. While not perfect downstream of the emitting regions, it avoids large numerical artifacts while providing much improved results everywhere else.

3.5 Radiating Spheres

As a last idealized test, we consider boosted radiating spheres on a comoving grid. That is, we consider spheres of radius $r_s = 0.5$ in which $\eta = \kappa_a = 1$ and $\kappa_s = 0$, then perform the coordinate transformation $t' = W(t - vx)$, $x' = x/W$, $y' = y$, $z' = z$, with $W = 1/\sqrt{1 - v^2}$ the Lorentz factor. In that frame, the emitting sphere is boosted, but the center of the sphere is comoving with the computational grid. The 3-metric is $\gamma_{ij} = \delta_{ij}$, the lapse $\alpha = 1$, and the shift $\beta^i = (v, 0, 0)$. This provides us with a good test of semi-transparent systems and Lorentz boosts. We consider $v = 0.1$ and $v = 1/\sqrt{2}$, and a grid spacing $\Delta x \sim 0.04$.

The larger velocity case is maybe the most interesting, because it causes problems both for the standard moment scheme with M1 closure and for our MC-Moments algorithm. We show the energy density of neutrinos for that test in Fig. 9, for simulations using the M1 closure, the pure MC closure, and the weighted average of the MC and M1 closure which we propose in this work. We see that the M1 closure performs surprisingly poorly in this test, with large overestimates of the energy density upstream of the emitting region. The total energy leaving the domain is, however, correct. The error in the M1 results is solely due to the improper interaction of neutrinos converging upstream of the sphere.

The pure MC closure, on the other hand, encounters some issues downstream of the emitting sphere. This is in fact the only test for which we find that a straightforward use of the MC closure does not produce acceptable results (for spheres boosted at a lower velocity, the MC closure performs well). We posit that this issue is due to the fact that the neutrino fluxes ($F_i, F_{i,MC}$) in the MC and M1 closure become inconsistent, and that error can accumulate in the region downstream of the emitting sphere because “trapped” modes exist there, i.e. the forward propagating mode coupling E and F_x on that axis has a vanishing characteristic speed on the grid at two points downstream of the emitting region, and is trapped in between those points. When using a pure MC closure, the Eddington tensor is independent of the evolution of the moment equations, and does not react to the build-up of an erroneous spike of energy downstream of the sphere.

In that region, however, the relative difference between the neutrino fluxes in the MC and moment evolution is of order unity. So with our weighted average of the M1 and MC closure, which uses the M1 closure when strong disagreements between the MC and M1 results are observed, we do have a feedback mechanism which prevents the accumulation of energy in that region. The evolution of the neutrino energy density in that region is inaccurate regardless of the scheme used, but this is also a region in which that energy density should be quite low. For the moment, we accept the weighting of the two closure methods as a necessary evil if we want to maintain numerical stability in this problem.

The lower velocity case, with $v = 0.1$, does not show the same dramatic errors as the large velocity case. As a less pathological case, it is useful to get a better handle on the accuracy and convergence properties of the code. We first consider two evolutions with the same grid spacing $\Delta x = 0.05$, but different number of packets. The first simulation uses ~ 20 packets per grid cell at the peak of the energy distribution, while the second uses ~ 80 pack-

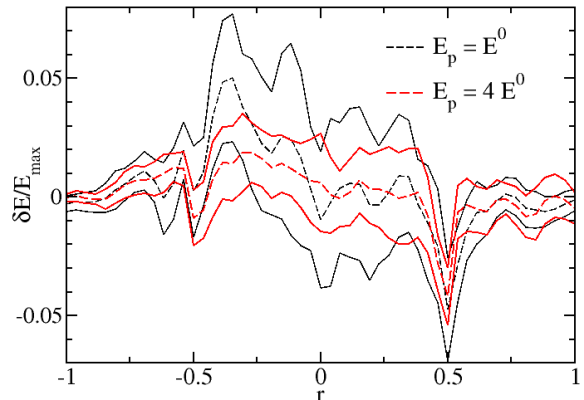


Figure 10. Error in the energy density of the neutrinos around an emitting sphere of radius $r_s = 0.5$ with a Lorentz factor $W = \sqrt{1.01}$, shown along the axis parallel to the direction of propagation of the sphere and passing through its center. The errors are normalized to the energy density at the center of the sphere. The thinner black curves and thicker red curves show results with a different number of MC packets, but the same resolution: the red curves have four times as many packets. Solid curves show $1 - \sigma$ deviations and dashed curves time-averaged values. We average over 50 simulation snapshots in the interval $t = [5, 10]$. The errors are relatively small, and using more packets provides the expected slow decrease in the statistical noise due to the use of MC methods.

ets per cell. The moments are averaged over $N_0 = 75$ and $N_0 = 300$ packets, and the two simulations thus use the same effective averaging timescale for the computation of the MC moments. The relative error in the average solution is shown on Fig. 10, together with the standard deviation in that solution. Averages are taken over 50 snapshots spaced by $\Delta t = 0.1$, starting at $t = 5$. In the region with the largest standard deviation, increasing the number of packets by a factor of 4 decreases statistical variations by roughly the expected factor of 2. Away from that region, the improvement is significantly slower. While there is a slight improvement in the average solution when increasing the number of packets, particularly at the edge of the emitting sphere, there is no reason to expect that the evolution should converge to the correct solution as the number of packets increases, as we keep the grid spacing constant.

We now consider simulations with different grid resolution: $\Delta x = (0.05 * 1.5, 0.05, 0.05/1.5)$. We also vary the number of packets on the grid as $(\Delta x)^{-3}$, which allows us to use $N_0 \propto (\Delta x)^{-1}$ while keeping the effective averaging timescale for the MC moments constant (we use $N_0 = 75$ for the medium resolution). This does not significantly reduce the statistical noise as the grid spacing decreases, but is fairly typical of the changes in packet number that we may be able to afford in astrophysical simulations. Relative errors for the average energy density, computed as for the previous test, are shown on Fig. 11. We see that the solution improves with resolution, albeit quite slowly. Given the significant noise introduced by the MC evolution, which is

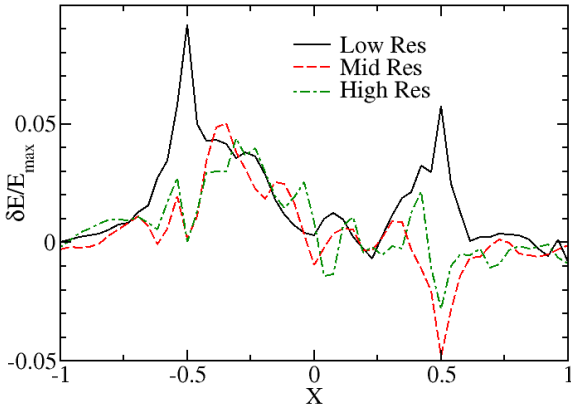


Figure 11. Error in the energy density of the neutrinos around an emitting sphere of radius $r_s = 0.5$ with a Lorentz factor $W = \sqrt{1.01}$, shown along the axis parallel to the direction of propagation of the sphere and passing through its center. The errors are normalized to the energy density at the center of the sphere. We show results for three resolutions, with grid spacing varying by a factor of 1.5 between each resolution. The number of MC packets on the grid scales as $(\Delta x)^{-3}$. While the solution certainly improves with resolution, noise from the MC evolution makes it impossible to derive an effective order of convergence.

at least comparable to the error due to finite grid spacing, a more rigorous study of the convergence of the solution would be a very challenging task. This points to a potential drawback of our algorithm: true convergence studies would require simulations with unrealistically large differences in the required computational resources. We will instead, at first at least, have to rely on the tests presented here, together with simulations varying a single parameter of the algorithm (e.g. E_p , N_0, \dots) to estimate errors.

3.6 Core-Collapse profile

Finally, we consider a test of the coupling of the MC-Moments evolution with the evolution of the temperature and composition of the fluid. We use a much more advanced setup, in which we evolve in 3D the post-bounce remnant of a core-collapse simulation from Ott et al. (2006). The result of the simulation is averaged into a 1D, spherically symmetric profile. In our test, we do not evolve the general relativistic equations of hydrodynamics, but modify the temperature and composition of the fluid as neutrinos are emitted and absorbed (the velocity of the fluid remains zero, and the metric is Minkowski). The same test has already been used by Abdikamalov et al. (2012), and to test our moment scheme with M1 closure (Foucart et al. 2015, 2016b). We use the equation of state from Shen et al. (1998), with 12 energy groups for the tabulated values of the neutrino emissivities and absorption coefficients. We also use a very coarse resolution $\Delta x \sim 6$ km, and neutrino packets of $E_p \sim 1.8 \times 10^{43}$ ergs. This results in $\sim 500 - 1000$ packets of each neutrino species leaving the computational grid over a time unit $t_g = GM_\odot/c^3 \sim 5 \mu\text{s}$, and $\sim 10^6$ packets per species on the grid at any given time.

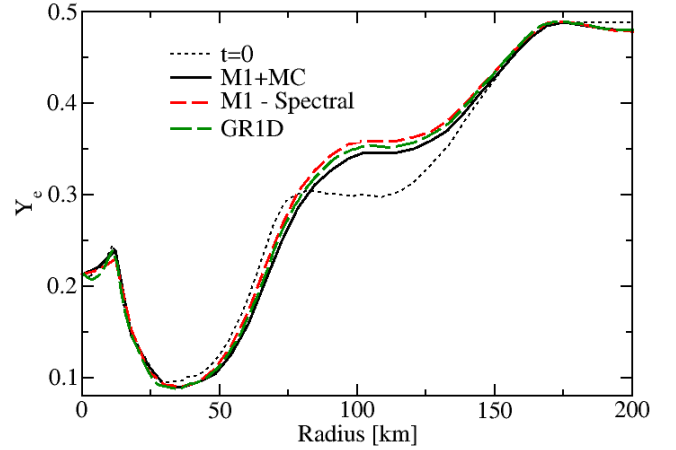


Figure 12. Composition of the fluid along the $x^2 = x^3 = 0$ axis, 8 ms into the evolution of a post-bounce core-collapse profile. We show results for our mixed MC-Moments algorithm, for our spectral M1 algorithm, and for the GR1D code.

The minimum averaging timescale used for the computation of the moments is $\tau_d = 2(1 + 0.1[r/r_g])t_g$, with $r_g = GM_\odot/c^2$.

The region close to the origin has high $\kappa_{a,s}$, and the heavy-lepton neutrinos have a large region with $\kappa_s \gg 1$, $\kappa_a \ll 1$. This test thus provides an interesting way to check whether the interface between optically thick regions and optically thin regions, which are treated differently in our MC-Moments scheme, results in any unphysical artifacts. We can also test that the evolution of the composition and temperature is consistent with previous simulations of this problem, and that the flux of MC packets leaving the grid is consistent with the outgoing flux in the moment evolution in a relatively complex setting.

We have verified that indeed, even in this coupled problem, the evolution of the MC and moment equations remain consistent, in the sense that the neutrino fluxes across the grid boundary are consistent within $\sim 10\%$ between the MC and moment evolutions. We also show on Fig. 12 the composition of the fluid 8 ms into the simulation. We compare the results of our new algorithm with an energy-dependent moment scheme using the M1 closure, and with a 1D simulations with the GR1D code (O'Connor & Ott 2010) which also uses an energy-dependent moment scheme with M1 closure, and has been compared with full transport simulations. We see good agreements between all the schemes, even though the evolution of the composition is known to be quite sensitive to small differences in the implementation of the transport equations (see e.g. the large variations between different iterations of the gray M1 scheme found in Foucart et al. 2015). The interface between the optically thick and optically thin regions does not cause any problem, as long as the time-averaging of the moments occurs on short timescales in regions with $\kappa_a \gtrsim 1$. This is guaranteed by our current scheme, as our damping timescale scales as the inverse of the number of packets crossing a cell. If we use instead a constant averaging timescale across the entire simulation, and that timescale is too long in optically thick regions (i.e. if $\tau_d \gtrsim \kappa_a^{-1}$), we find that the evolution of the composition in these regions is numerically unstable.

We find that for this test problem, the energy-dependent moment formalism with M1 closure agrees with our more advanced transport scheme within $\sim (10 - 20)\%$ for the luminosity and average energy of the neutrinos, except for the luminosity of heavy-lepton neutrinos which is a factor of ~ 1.6 larger when using the M1 closure. As the energy spectrum of heavy-lepton neutrinos is consistent between simulations, the MC and moment evolution provide consistent results in our simulation, and the evolution of the temperature is also in good agreement in all three simulations, it is unclear at this point what differences in the setup of the test may explain this. The approximate treatment of high- κ_s regions would be a natural explanation for discrepancies in the heavy-lepton luminosity, but, if wrong, it should affect the neutrino spectrum and cause disagreements between the neutrino fluxes measured in the moments and MC algorithms. An other indication that these regions are not to blame is that we performed a simulation in which we treated scatterings exactly down to $\kappa_s \Delta \tau = 10$ and evolved packets down to opacities $\kappa_{\text{crit}} = 20$. That simulation was consistent with the results of our standard configuration, within a few percents. Decreasing the grid spacing by a factor of 2 led to differences at the $\sim 10\%$ level only. Considering that the high- κ_s regions which are so important in setting the characteristics of the heavy-lepton neutrinos are also particularly difficult to capture for all schemes involved, it is likely that only a more dedicated comparison with a full transport code would allow us to determine what difference in the setup of the test explains this one remaining discrepancy.

Overall, this test provides encouraging indications that our mixed MC-Moments scheme can be used in the simulation of astrophysical systems. We also note that, even if the MC evolution is more expensive than the gray moment scheme, at the small number of packets used in this simulation its cost is comparable to the energy-dependent moment scheme! This is despite the fact that the main drawback of the energy-dependent moment scheme, i.e. the potential presence of large energy fluxes in energy space, is not tested by this evolution in which the fluid velocity vanishes everywhere, and the metric is Minkowski. Additionally, nearly all MC packets are owned by the processor on which we evolve the region closest to the center of the neutron star. With a more optimized parallelization of MC packets, the coupled MC-Moments algorithm would presumably be cheaper than the energy-dependent moment scheme in this specific problem and for the low-resolution MC evolution used here.

4 CONCLUSIONS AND PROSPECTS

In this work, we show that the evolution of the general relativistic equations of radiation transport using the moment formalism can be complemented by a low-accuracy Monte-Carlo evolution, from which any information required to close the evolution equations of the moments can be extracted. In our algorithm, it is sufficient to evolve MC packets in regions of low absorption optical depth, which avoids many of the more complex and costlier steps of MC radiation transport. We also use time-averaged information from the MC evolution to close the evolution equations for the moments, thus reducing at will the number of MC packets necessary to obtain accurate closure relations. We im-

plement this algorithm in the general relativistic hydrodynamics code SpEC, and test our implementation on both simple problems demonstrating that the code properly captures the equations of radiation transport, and on a more complex test coupling the evolution of the radiation to the temperature and composition of the fluid. For this first study of the coupled MC-Moments algorithm, we do not consider full coupling to the evolution of the metric and/or the fluid equations.

Our tests indicate that the coupled MC-Moments evolution always performs better than the more standard approximate M1 closure, and properly reproduces known analytical solutions even for configurations in which the M1 closure fails spectacularly. The coupling of the two systems of equations has to be treated carefully, in order to avoid the growth of numerical instabilities. Accordingly, we provide a detailed description of the steps taken in our current implementation to avoid such instabilities, and of the tests for which simpler methods fail. We also show that regions of high-scattering opacities can be treated approximately, to avoid the large cost of propagating MC packets through many scatterings, but only as long as the momenta of neutrino packets at the end of such approximate evolution are drawn from a distribution fitted to the result of more detailed scattering experiments. While our method to choose the momentum of the packets introduces additional complexity in the MC algorithm, it does not significantly alter the cost of the evolution.

The coupled MC-Moments algorithm has a number of potential applications in the study of astrophysical systems in which neutrino and photon transport play an important role. It can be used either to obtain the distribution function of neutrinos/photons in time-independent snapshots of a more complex general relativistic hydrodynamics simulation, or can be directly coupled to such evolution. The time averaging of the moments, and the flexibility in the choice of regions within which MC packets are evolved (as opposed to regions in which we assume a thermal distribution of neutrinos/photons when computing closure relations) make it fairly easy to adapt the level of accuracy of the transport scheme to the computational resources available for any given simulation. But its main advantage may be that it actually converges, albeit slowly, to a true solution of Boltzmann's equation. It can also provide a first step towards more expensive, purely MC schemes.

We now expect to use our algorithm first on time-independent snapshot of neutron star merger simulations and then, as computationally possible, in merger simulations in which our MC-Moments scheme is fully coupled to the evolution. There is a lot of information to glean at each of these steps about the impact of neutrinos on observable properties of mergers. Even evolutions on time-independent simulation snapshots would provide greatly improved estimates of the amount of energy deposition in low-density regions by $\nu\bar{\nu}$ pair annihilation, as well as a new method to test the accuracy of more approximate schemes and to extract reliable information about the spectrum of neutrinos and their detailed distribution function. The latter may be particularly useful in the study of neutrino oscillations in neutron star mergers.

Fully coupled evolutions would, of course, be even more useful. Large uncertainties in the composition of the out-

flows produced by neutron star mergers, which is set by neutrino-matter interactions, remain a significant roadblock in the production of reliable models for the electromagnetic transients powered by these mergers and for the outcome of r-process nucleosynthesis in that ejecta. Additionally, the deposition of energy by $\nu\bar{\nu}$ pair annihilation feeds back on the evolution of the matter, and could impact the ability of neutron star mergers to power short gamma-ray bursts.

While moving from the relatively idealized test problems presented in this work to merger simulations is not a simple task, particularly if one wants to make sure that the computations required by the MC algorithm are optimally distributed on the available computational resources, our results are quite encouraging for coupled MC-Moments algorithms. The radiation transport scheme presented here does not require any modification of the general relativistic hydrodynamics code currently used by SpEC, so that most impact of the use of a new radiation scheme have in fact been tested in this work. The work required to move to more realistic astrophysical systems is dominated by the necessity to optimize the implementation of the algorithm, and by the determination of the level of approximation that remains acceptable in the evolution of MC packets in more complex systems: which regions of the simulation can be ignored by the MC algorithm, and how long of an averaging timescale can we use for the moments without creating unphysical artifacts in the simulation.

ACKNOWLEDGEMENTS

The author wish to thank Daniel Kasen and Jennifer Barnes for useful discussions about the use of Monte-Carlo methods in radiation hydrodynamics simulations, as well as Eliot Quataert, Matthew Duez, Sherwood Richers and Ben Ryan for their comments and suggestions. The author also wish to thank the attendees of the MICRA conference at Michigan State University and of the INT workshop “Electromagnetic Signatures of R-process Nucleosynthesis in Neutron Star Binary Mergers” for stimulating discussions related to this work. Support for this work was provided by NASA through Einstein Postdoctoral Fellowship grants numbered PF4-150122 awarded by the Chandra X-ray Center, which is operated by the Smithsonian Astrophysical Observatory for NASA under contract NAS8-03060

REFERENCES

- Abdikamalov E., Burrows A., Ott C. D., Loffler F., O’Connor E., Dolence J. C., Schnetter E., 2012, *Astroph.J.*, **755**, 111
- Barnes J., Kasen D., 2013, *Astroph.J.*, **775**, 18
- Davis S. W., Stone J. M., Jiang Y.-F., 2012, *Astroph.J.Suppl.*, **199**, 9
- Deaton M. B., et al., 2013, *Astrophys. J.*, **776**, 47
- Duez M. D., Foucart F., Kidder L. E., Pfeiffer H. P., Scheel M. A., Teukolsky S. A., 2008, *Phys.Rev.D.*, **78**, 104015
- Foucart F., et al., 2013, *Phys. Rev. D*, **87**, 084006
- Foucart F., et al., 2015, *Phys.Rev.D.*, **91**, 124021
- Foucart F., et al., 2016a, *Phys.Rev.D.*, **93**, 044019
- Foucart F., O’Connor E., Roberts L., Kidder L. E., Pfeiffer H. P., Scheel M. A., 2016b, *Phys.Rev.D.*, **94**, 123016
- Fujibayashi S., Sekiguchi Y., Kiuchi K., Shibata M., 2017, preprint, ([arXiv:1703.10191](https://arxiv.org/abs/1703.10191))
- Harten A., Lax P. D., van Leer B., 1983, *SIAM Review*, **25**, 35
- Hughes S. A., Keeton II C. R., Walker P., Walsh K. T., Shapiro S. L., Teukolsky S. A., 1994, *Phys.Rev.D.*, **49**, 4004
- Jiang G.-S., Shu C.-W., 1996, *Journal of Comp.Phys.*, **126**, 202
- Jin S., Levermore C. D., 1996, *J. Chem. Phys.*, **126**, 449
- Just O., Obergaulinger M., Janka H.-T., 2015, *MNRAS*, **453**, 3386
- Kasen D., Badnell N. R., Barnes J., 2013, *Astroph.J.*, **774**, 25
- Korobkin O., Rosswog S., Arcones A., Winteler C., 2012, *MNRAS*, **426**, 1940
- Lattimer J. M., Schramm D. N., 1976, *Astroph.J.*, **210**, 549
- Li L.-X., Paczynski B., 1998, *Astroph.J.*, **507**, L59
- Lippuner J., Roberts L. F., 2015, *Astroph.J.*, **815**, 82
- Liu X.-D., Osher S., Chan T., 1994, *Journal of Comp.Phys.*, **115**, 200
- Minerbo G. N., 1978, *J.Quant.Spec.Radiat.Transf.*, **20**, 541
- Nagakura H., et al., 2017, preprint, ([arXiv:1702.01752](https://arxiv.org/abs/1702.01752))
- Neilsen D., Liebling S. L., Anderson M., Lehner L., O’Connor E., Palenzuela C., 2014, *Phys.Rev.D.*, **89**, 104029
- O’Connor E., Ott C. D., 2010, *Class.Quant.Grav.*, **27**, 114103
- Ott C. D., Burrows A., Dessart L., Livne E., 2006, *Phys.Rev.Lett.*, **96**, 201102
- Perego A., Cabezón R. M., Käppeli R., 2016, *ApJ Suppl.*, **223**, 22
- Perego A., Yasin H., Arcones A., 2017, *Journal of Physics G Nuclear Physics*, **44**, 084007
- Radice D., Galeazzi F., Lippuner J., Roberts L. F., Ott C. D., Rezzolla L., 2016, *MNRAS*, **460**, 3255
- Richers S., Nagakura H., Ott C. D., Dolence J., Sumiyoshi K., Yamada S., 2017, preprint, ([arXiv:1706.06187](https://arxiv.org/abs/1706.06187))
- Roberts L. F., Kasen D., Lee W. H., Ramirez-Ruiz E., 2011, *Astrophys. J. Lett.*, **736**, L21
- Roberts L. F., Ott C. D., Haas R., O’Connor E. P., Diener P., Schnetter E., 2016, *Astroph.J.*, **831**, 98
- Roth N., Kasen D., 2015, *Astroph.J.Suppl.*, **217**, 9
- Ryan B. R., Dolence J. C., Gammie C. F., 2015, *Astroph.J.*, **807**, 31
- Shen H., Toki H., Oyamatsu K., Sumiyoshi K., 1998, *Nuclear Physics A*, **637**, 435
- Shibata M., Kiuchi K., Sekiguchi Y., Suwa Y., 2011, *Progress of Theoretical Physics*, **125**, 1255
- Thorne K. S., 1981, *MNRAS*, **194**, 439
- Wanajo S., Sekiguchi Y., Nishimura N., Kiuchi K., Kyutoku K., Shibata M., 2014, *Astrophys.J.Lett.*, **789**, L39

This paper has been typeset from a $\text{\TeX}/\text{\LaTeX}$ file prepared by the author.